

*Chapter 9*

**MAGNETIC RECONNECTION IN THE EARTH'S  
MAGNETOTAIL: RECONSTRUCTION METHOD  
AND DATA ANALYSIS**

*T. Penz*<sup>1,2\*</sup>, *V. V. Ivanova*<sup>3</sup>, *V. S. Semenov*<sup>3</sup>, *R. Nakamura*<sup>1</sup>,  
*I. B. Ivanov*<sup>4,5</sup>, *H. K. Biernat*<sup>1,2</sup>, *M. F. Heyn*<sup>4</sup>, *V. A. Sergeev*<sup>3</sup>,  
*and I. V. Kubyshkin*<sup>3</sup>

<sup>1</sup> Space Research Institute, Austrian Academy of Sciences,  
Schmiedlstr. 6, A-8042 Graz, Austria

<sup>2</sup> Institute of Physics, University of Graz, Universitätsplatz 5,  
A-8010 Graz, Austria

<sup>3</sup> Institute of Physics, State University St. Petersburg, 198504 Russia

<sup>4</sup> Institute for Theoretical Physics, Technical University Graz,  
Petersgasse 16, A-8010 Graz, Austria

<sup>5</sup> Petersburg Nuclear Physics Institute, Gatchina, 188300 Russia

**Abstract**

Magnetic reconnection is a topological restructuring of magnetic field lines, leading to a conversion of magnetic energy into kinetic energy and a heating of the plasma. It takes place in regions with strong magnetic gradients: the Earth's magnetopause and the plasma sheet in the magnetotail, during solar and stellar flare events, and in laboratory plasmas on the Earth. It is also involved in astrophysical phenomena like the generation of relativistic jets and processes in accretion disks. The Earth's magnetosphere is the only region where signatures of magnetic reconnection can be measured in-situ by satellites. Based on the method developed by Semenov et al. [1], we solve the direct problem of magnetic reconnection and calculate the magnetic field and plasma flow disturbances in a compressible plasma caused by transient reconnection. In order to get the reconnection rate from measured data, we invert the problem. Since the inverse problem is ill-posed, it is treated with the method of regularization. Application of this method to Cluster measurements from September 8<sup>th</sup>, 2002, where a series of Earth-ward propagating 1-minute scale magnetic field and plasma flow variations were observed outside of the plasma sheet, showed good agreement for the z-component of

---

\*E-mail address: thomas.penz@oeaw.ac.at

the reconstructed magnetic field. The reconnection rate is about 1 mV/m and the reconnection region is located at about 24–25 Earth radii in the magnetotail.

**Keywords:** Magnetic reconnection, Magnetotail, Cluster, Magnetohydrodynamics

## 1. Introduction

Magnetic reconnection is a fundamental plasma process allowing the conversion of magnetic energy into kinetic and thermal energy of the plasma. The occurrence of thin current layers associated with a plasma flow and the presence of magnetic fields inevitably leads to the process of magnetic reconnection. In fact, magnetic reconnection is caused by a change in the plasma resistivity leading to the release of stored magnetic energy.

On scales larger than the characteristic length of the plasma (e.g., the gyroradius), the motion of the plasma is coupled with the magnetic field. This is called the frozen-in condition, which implies that plasma and magnetic fields from distinct regions do not intermix and stay separated. In the upper panel of Fig. 1, this situation is displayed for the simple configuration of two antiparallel magnetic fields, which are kept apart by a thin current layer. If magnetic flux is added to the current sheet from both sides, free energy is accumulated in the current sheet. After some time, the gradients across the current sheet become too strong, resulting in a violation of the frozen-in condition. If such a violation takes place, reconnection is initiated.

Because of the highly non-uniform structure of the current sheet, it is very likely that a local breakdown of the frozen-in condition takes place, leading to the formation of the so-called diffusion region. Early models of magnetic field annihilation as proposed by Sweet [2] and Parker [3] assumed a diffusion region with a size comparable to the whole current sheet. It was quickly realized that this process is much too slow to account for rapid energy release expected in many astrophysical processes. A way to avoid this problem was proposed by Petschek in 1964 [4]. In contrast to the Sweet–Parker model, where homogeneous resistivity is assumed, Petschek proposed a localized enhancement of the resistivity in a highly conducting fluid. Thus, the diffusion region, where the assumption of an ideal conducting plasma does not hold, becomes much smaller than the scale size of the system (the black area in the middle panel of Fig. 1). Petschek showed that the diffusion region is the source for large amplitude MHD waves. In this model, most of the inflowing plasma crosses the shock waves and not the diffusion region anymore. From this point of view, the shock waves transport information into a wide region of ideal plasma, allowing for much higher reconnection rates than in the Sweet–Parker model. It was also shown by simulations using resistive MHD equations that the Sweet–Parker configuration appears for a spatially constant plasma resistivity, while Petschek-type structures arise for a strongly localized plasma resistivity [5, 6]. This insight is also supported by numerical simulations [7]. The newly formed region bounded by the shock waves is called outflow region, where the inflowing plasma is heated and accelerated, leading to the formation of bi-directional jets [8] and fast plasma flows, which are important features indicating the occurrence of magnetic reconnection. Also the connection of the magnetic field lines takes place over the outflow region (lower panel of Fig. 1).

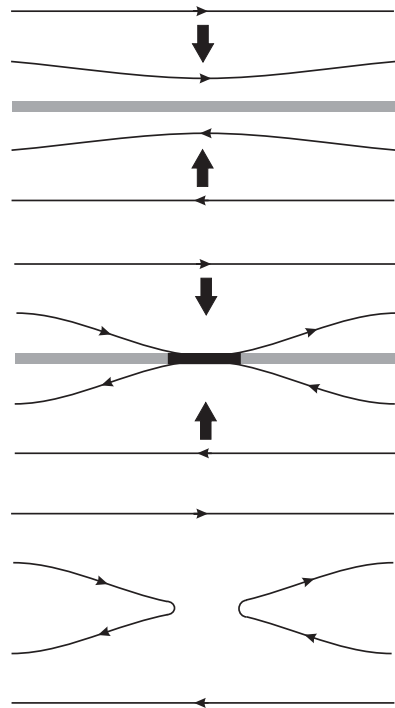


Figure 1. Different stages during the process of magnetic reconnection. The upper panel shows the initial configuration of antiparallel magnetic fields separated by a thin current sheet (dashed area). If the magnetic fields are convected towards each other, strong gradients occur, leading to the formation of a diffusion region (black area), where the frozen-in condition is not valid anymore (middle panel). In this region, the magnetic field lines can be broken and reconnected (lower panel). This leads to a connection between plasma regions which were previously separated.

In the last century, many sites were discovered where magnetic reconnection plays a crucial role [9]. It is observed in laboratory fusion machines like tokamaks [10, 11]. In order to investigate the fundamental physics involved in magnetic reconnection in laboratory settings, different devices like the Magnetic Reconnection Experiment (MRX) device were constructed [12]. It revealed the appearance of different shapes of the diffusion region as well as the importance of the shear angle between the magnetic field lines and the influence of boundary effects.

Moving away from the Earth, other plasma environments suitable for reconnection can be found. The first environment where magnetic reconnection was expected is the Sun. The earliest models [13, 2] have aimed at explaining the large amount of energy released in solar flares. Reconnection on the Sun is inferred from different observations, including high speed flows of X-ray and EUV features, and energetic particle events in hard X-ray images [14, 15], which have been observed by several spacecrafts like Yohkoh, SOHO, and TRACE. The application of Petschek-like reconnection to solar flares gives typical recon-

nection times consistent with observations [16]. Reconnection has also been proposed as a mechanism for the heating of solar and stellar coronae to extremely high temperatures of more than  $10^6$  K [17]. The importance of reconnection in plasma environments outside of our solar system is still under debate. The two astrophysical topics to which reconnection theory has been extensively applied are stellar flares [18] and accretion disks [19]. Reconnection theory also enters into models of protostellar collapse, extragalactic jets, galactic magnetic fields, and even galactic clusters [9].

However, the only place in space where magnetic reconnection can be observed in-situ is the terrestrial magnetosphere. At the dayside magnetopause, energy and plasma from the solar wind can enter the terrestrial magnetosphere because of the reconnection of the interplanetary magnetic field (IMF) and the Earth's magnetic field [20]. Of particular interest is the transient feature of magnetic reconnection, leading to the formation of so-called flux transfer events (FTEs), which are flux tubes connecting the solar wind plasma with the magnetospheric plasma. The first in-situ measurements of flux transfer events caused by transient reconnection were reported by Russell and Elphic in 1978 [21] for the dayside magnetopause. They defined FTEs as signatures with a bipolar variation of the magnetic field component perpendicular to the current sheet, a deflection of the tangential component, and an increase in the magnetic field strength. In the same year, Haerendel et al. [22] found indications for reconnection processes also at the high-latitude dayside magnetopause. In the following years, a collection of studies supported the interpretation that FTEs are bursts of magnetic reconnection at the magnetopause appearing most frequently during intervals of southward directed IMF [23, 24]. However, newer observations with the Cluster satellites show that for a northward-orientated IMF, reconnection can appear tailward of the cusp [25]. There are also strong indications that reconnection at the dayside magnetopause can be continuous over an extended period of time [26].

Magnetic flux reconnected at the dayside is convected into the tail lobes, where reconnection is initiated in a region between 15 and 30  $R_e$  in the magnetotail [27, 28]. It was proposed by Sergeev et al. [29] that FTE-like structures appear also in the Earth's magnetotail. They performed a qualitative comparison between measurements of ISEE-1 and model predictions from a transient reconnection model, which showed a general agreement. In later work, these events were referred to as nightside flux transfer events (NFTEs) [30]. These are short-term events in the substorm-time plasma sheet, which can be described by impulsive variations of the reconnection rate in models of transient reconnection. They are characterized, similar to FTEs, as a bipolar variation of the  $B_z$ -component and a deflection of the  $x$ -component of the magnetic field. Additionally, the velocity shows an upward flow of plasma in the beginning, followed by a strong flow directed downward to the current sheet. Such structures noticed in the tail plasma sheet are often referred to as individual bursts of BBF, as transient plasma sheet expansions, as plasmoids or flux ropes, as well as NFTEs [30, 31, 32]. The appearance of reconnection structures in the magnetotail was also confirmed by several other satellite missions, like Geotail [33] or Cluster [34, 35].

The aim of this paper is to show recent evidence for magnetic reconnection from Cluster measurements and introduce a model for the reconstruction of the reconnection rate from satellite measurements. In Section 2, multi-spacecraft measurements of the Cluster mission are discussed with emphasize to the implications for magnetic reconnection. The theoretical model used to analyze NFTEs in the terrestrial magnetotail is described in Section 3. Sec-

tion 4 is devoted to the reconstruction of the reconnection rate from Cluster measurements. Also the site of reconnection with respect to the satellite is estimated.

## 2. Observational Features of Magnetotail Reconnection

Whereas the dayside magnetosphere is compressed by the solar wind, the nightside magnetosphere is stretched out into a long magnetotail. When the interplanetary magnetic field (IMF) is southward, the merged field lines at the dayside are transported towards the nightside, reconnected in the distant tail and then transported back towards the dayside, creating inward and Earthward flows in the central plasma sheet. The flux transport rates at the dayside and at the nightside are, however, balanced only in an average sense and the unbalanced transport is the ultimate cause of a substorm when magnetic reconnection takes place closer to the Earth, at radial distance of 15 - 30  $R_E$  in the tail. The processes associated with this near-Earth reconnection determine different scales of magnetotail dynamics.

Cluster traversed the magnetotail covering regions Earthward of 19  $R_E$  during the past summer seasons since July 2001. The tetrahedron scale was between 250 km and 4000 km, which was changed every year, so that characteristics at different scales could be identified. The four spacecraft observations enable us for the first time to differentiate spatial from temporal disturbances. In this section, we highlight several Cluster observations when Cluster was located near the X-line and more remote observations showing the effects of the processes in the ion diffusion region.

### 2.1. Observation near the X-line

The four spacecraft observations enable us to obtain spatial gradients of different parameters continuously. For example, the current density obtained from the gradient in the magnetic field is an essential parameter for magnetotail diagnostics. Using the gradient information obtained from the four Cluster spacecraft during current sheet crossings, current sheet structures in the vicinity of X-line were reconstructed by Runov et al. [34] as illustrated in Fig. 2. A thin current sheet with a half-thickness of about one ion gyro radius was found for the crossing closest to the X-line, whereas the outer crossings showed bifurcated current sheet profiles. Changes in the curvature of the field for the different current sheet crossings illustrated in the figure were consistent with a X-line motion from Earthward and tailward of the spacecraft. Furthermore, consistent features of the field disturbance associated with Hall-current at both side of X-line were identified, confirming that the spacecraft traversed the ion diffusion region.

The importance of multi-scale processes from heavy ions to electron kinetics in the reconnection processes have been identified by several Cluster observations. During thin current sheet intervals associated with crossings of the X-line during storm-time substorms, the  $O^+$  pressure and density were observed to be dominated compared to those of  $H^+$  [36]. In such current sheets, the  $O^+$  were observed to execute Speiser-type serpentine orbits across the tail and were found to carry about 5-10% of the cross-tail current [36]. The  $O^+$  in the reconnection region was suggested to experience a ballistic acceleration [37] based on the observation of a large amplitude bipolar electric field. These large-amplitude

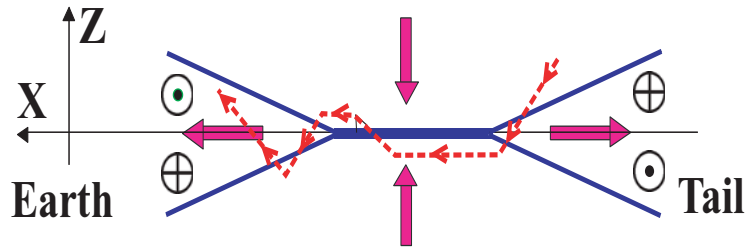


Figure 2. Sketch of Cluster observations of Hall magnetic fields and current sheet structure around the reconnection region; the red dashed line indicates the trajectory of Cluster (after Runov et al. [34]).

(up to 50 mV/m) solitary waves, identified as electron holes, have been observed during several plasma sheet encounters that have been identified as the passage of a magnetotail reconnection X-line [38]. The electron holes were seen near the outer edge of the plasma sheet, within and on the edge of a density cavity, at distances in the order of a few ion inertial lengths from the center of the current sheet. Based on a detailed comparison with simulations, Cattell et al. [38] suggested that the observed nonlinear wave modes, electron holes, may play an important role in reconnection by scattering and energizing electrons.

## 2.2. Observations Away from the Reconnection Site

Whereas in situ observations of the ion diffusion region depend on the rare chance that the spacecraft being located at the right place at the right time, different effects of reconnection can be detected remotely from the reconnection site and can still contain useful information on temporal and spatial characteristics of reconnection. For example, the limited area of the Hall currents flowing in the ion diffusion region indicates that the current has to be closed including regions outside of the ion diffusion region. At the lobe side, the closure of the Hall current takes place via cold electron flowing into the ion diffusion region. At the outflow region, on the other hand, the accelerated electrons can carry the current into the ion diffusion region. Cluster observed such field-aligned electrons related to the Hall current system consistent with previous observations, but also obtained fine structures indicating multiple temporal or spatial properties of reconnection [39, 40, 41]. Fig. 3 illustrates multi-point observations by Cluster in the northern hemisphere and by Geotail in the southern hemisphere detecting these field aligned currents possibly connected to the ion diffusion region from Nakamura et al. [39]. The four Cluster satellites also allowed to determine the scale size of these field aligned currents, suggesting that the scale size of the downward current was at maximum comparable to the ion inertia length so that it plausibly connects to the near-Earth X-line and is driven by Hall effects in the reconnection region. This interhemispheric observation supported the theoretical prediction [42] that the downward current region is thin because on the lobe side, the ions may travel a substantial fraction of the ion inertia length until their motion separates from that of the electrons.

Using multi-composition plasma observation by Cluster, slow-mode shocks connected

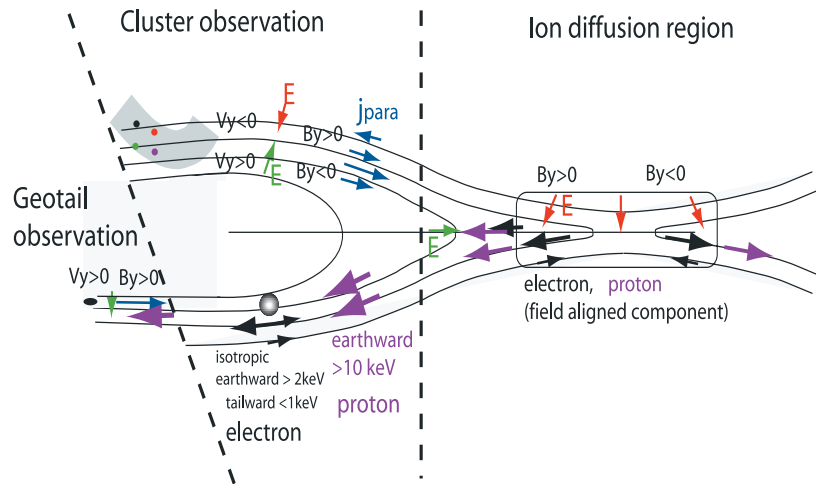


Figure 3. Summary of observations by Cluster and Geotail during a transient entry into the plasma sheet during a substorm event and illustration of the possible relationship to the reconnection region. For Cluster observations field signatures are showing in the northern hemisphere, while particle signatures are illustrated in the southern hemisphere; adapted from [39].

to the ion diffusion region have been analyzed by Eriksson et al. [43] taking into account also the contribution from oxygen ions during a substorm X-line event when Cluster observed fast tailward and Earthward flows. The successful joint Walén and slow shock analyses on the tailward flows within the plasma sheet presented further evidence in favor of Petschek-type reconnection at distances  $X_{GSM} > -19 R_E$  of the near-Earth magnetotail. Cluster succeeded to obtain detailed characteristics of Earthward propagating southward then northward magnetic field disturbances related to plasmoids/flux ropes [44, 45], travelling compression regions [46, 47], and nightside flux transfer events [48, 49, 35]. Multi-point analysis by Cluster were used to measure the current density and check the force-free model [46] and energetic particle boundaries [45] to show the structures of the plasmoid/flux rope. Yet, since the plasma flows jetting towards the Earth are significantly influenced by the strong dipolar field and pressure gradient, it still remains unknown to what extent these structures can be treated as motions of a stable structure in the analysis. As described in the later sections, similar magnetic features were rather interpreted as transient profiles of a remote X-line due to its change in the reconnection rate and used to determine the location of the X-line [48, 49, 35]. Observationally, the determination of the field topology would be a key to differentiate whether these structure are coming from a single X-line or are signatures of multiple X-lines.

In the plasma sheet, bursty bulk flows (BBF) are the most clear signatures of the consequence of reconnection and have been intensively studied using Cluster spacecraft measurements based on multi-point data analysis. A statistical analysis was performed by Nakamura et al. [50] to estimate the typical scale size of BBF. Different types of magnetic field disturbances accompanied by the BBF were studied such as dipolarization [51], low frequency

wave activity [52], and turbulence [53]. Using Cluster, together with the other spacecraft and ground-based observations, BBF-associated field-aligned and ionospheric current system have been obtained [54, 55].

### 3. The Petschek–Type Model of Magnetic Reconnection

In the following, we present a model to reconstruct the reconnection rate developed by Semenov et al. [67] for an incompressible plasma extended to a compressible one. First we show the solution of the direct problem, giving the behavior of NFTEs for a prescribed reconnection rate. To reconstruct the reconnection rate, we solve the inverse problem. This enables us to achieve the reconnection rate from magnetic field measurements.

#### 3.1. Basic Configuration

In order to describe the temporal evolution of FTEs, time–dependent Petschek–type models of reconnection were developed [1, 56, 57, 58, 59]. For our purpose, we consider the structure of the Earth’s magnetotail as oppositely directed magnetic fields, which are separated by a current sheet, the so–called plasma sheet. In terms of ideal MHD, this current sheet can be described as an infinitely thin tangential discontinuity. The normal components of the magnetic field and plasma velocity are zero ( $B_n = 0$ ,  $v_n = 0$ ) across a tangential discontinuity, while the density and the tangential components of the magnetic field and velocity can change arbitrarily, subject only to the requirement that the total pressure, which is the sum of the thermal and the magnetic pressure,  $p + B^2/(8\pi)$ , stays constant [60]. Due to these requirements, there is no mass flow and no magnetic connection across a tangential discontinuity. As a result, there will be no electric field component along the discontinuity ( $E_t = 0$ ).

Due to the local enhancement of the plasma resistivity, a tangential electric field is generated, causing a normal component of the magnetic field. Thus, the conservation laws for a tangential discontinuity are violated, and the surface gets non–linearly unstable, decaying into a system of MHD wave modes according to the general Riemann problem [61, 60]. The most general scheme of a decay looks like  $S^+(R^+)AS^-(R^-)C(T)S^-(R^-)AS^+(R^+)$ , where  $S^+$ ,  $S^-$  are fast and slow shocks,  $R^+$ ,  $R^-$  are fast and slow rarefaction waves, and A, C, T are Alfvén, contact, and tangential discontinuities, respectively. If we assume that the total pressure is conserved in lowest order, no strong fast shocks are present in the system. For symmetric conditions, no contact discontinuity and no rarefaction waves will appear. Due to this process, reconnection–associated disturbances start to propagate along the current sheet in the form of pairs of shocks. Until the reconnection electric field ceases, the shocks are detached to the reconnection site forming a teardrop–shaped region of heated and accelerated plasma, the so–called outflow regions (shaded areas in Fig. 4).

After the electric field has dropped to zero, the shocks detach from the reconnection site and continue to propagate along the current sheet (Fig. 4). These propagating shocks are causing disturbances in the ambient plasma environment, which can be measured by a satellite. In the following, we will show how these measured disturbances can be calculated by using a time–dependent Petschek–type model of transient magnetic reconnection.

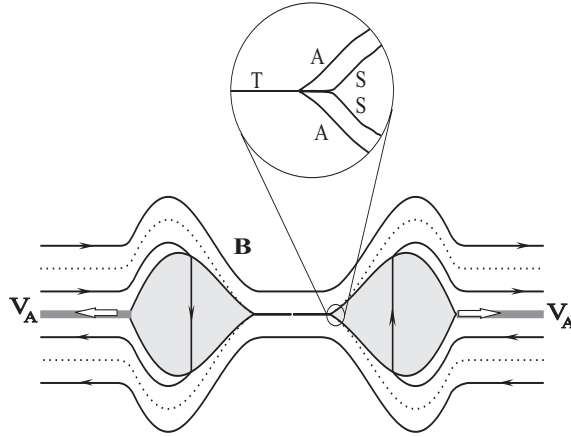


Figure 4. Shocks propagating away from the reconnection site with local Alfvén velocity. The small figure shows the internal structure of the shocks according to the general Riemann problem, where the tangential discontinuity decays into a slow shock  $S$  and an Alfvén wave  $A$ . The shaded areas are the so-called outflow regions.

### 3.2. MHD Treatment of the Problem for a Compressible Plasma

After the local reconnection of magnetic flux according to the Petschek-type model of magnetic reconnection, the plasma and magnetic field behavior in the outer regions can be described within the frame of ideal magnetohydrodynamics [1, 61],

$$\frac{\partial \rho}{\partial t} + \nabla \cdot (\rho \mathbf{v}) = 0, \quad (1)$$

$$\frac{\partial (\rho \mathbf{v})}{\partial t} + \nabla \cdot \left[ \rho \mathbf{v} \mathbf{v} + p \mathbf{I} - \frac{1}{4\pi} \left( \mathbf{B} \mathbf{B} - \frac{B^2}{2} \mathbf{I} \right) \right] = 0, \quad (2)$$

$$\frac{\partial}{\partial t} \left( \frac{\rho v^2}{2} + \rho e + \frac{B^2}{8\pi} \right) + \nabla \cdot \left[ \rho \mathbf{v} \left( \frac{v^2}{2} + e + \frac{p}{\rho} \right) + \frac{1}{4\pi} \mathbf{B} \times (\mathbf{v} \times \mathbf{B}) \right] = 0, \quad (3)$$

$$\frac{\partial \mathbf{B}}{\partial t} + \nabla \cdot (\mathbf{B} \mathbf{v} - \mathbf{v} \mathbf{B}) = 0. \quad (4)$$

These equations describe the conservation of mass (Eq. 1), momentum (Eq. 2), energy (Eq. 3), and magnetic flux (Eq. 4), respectively.  $\rho$ ,  $\mathbf{v}$ ,  $\mathbf{B}$ ,  $p$ , and  $e$  are the mass density, the plasma velocity, the magnetic field, the isotropic pressure, and the internal energy, respectively, and  $\mathbf{I}$  is the unit dyadic.

These ideal MHD equations can be linearized with respect to constant background quantities, in the following denoted by superscript (0). The linearization allows for the description of all first order quantities (indicated by superscript (1)) in terms of a displacement vector  $\xi$ ,

$$\mathbf{v}^{(1)} = \left( \frac{\partial}{\partial t} + \mathbf{v}^{(0)} \cdot \nabla \right) \xi, \quad (5)$$

$$\mathbf{B}^{(1)} = \mathbf{B}^{(0)} \cdot \nabla \xi - \mathbf{B}^{(0)} \nabla \cdot \xi, \quad (6)$$

$$\rho^{(1)} = -\rho^{(0)} \nabla \cdot \xi, \quad (7)$$

$$p^{(1)} = c_S^2 \rho^{(1)}, \quad (8)$$

$$P^{(1)} = -\rho^{(0)} [u^2 \nabla \cdot \xi + (\mathbf{v}_A \cdot \nabla) \mathbf{v}_A \cdot \xi]. \quad (9)$$

Here,  $P^{(1)}$  is the first order total pressure, while  $\mathbf{v}_A$  and  $c_S$  are the Alfvén velocity and the sound speed, respectively, and  $u^2 = v_A^2 + c_S^2$ .

Substituting these expressions (Eq. 5–9) into the linearized MHD equations, applying a Laplace transformation with respect to time  $t$ , and a Fourier transformation with respect to the spatial coordinate  $x$ , the  $z$ -component of the displacement vector  $\zeta(p, k, z)$  fulfills the ordinary differential equation

$$\frac{\partial^2}{\partial z^2} \zeta - q^2(p, k) \zeta = 0, \quad (10)$$

with

$$q^2 = \frac{p^4 + u^2 k^2 p^2 + v_A^2 c_S^2 k^4}{p^2 u^2 + v_A^2 c_S^2 k^2}. \quad (11)$$

The solutions of Eq. 10 which satisfy the first order total pressure balance at  $z = 0$  and vanish at infinity are

$$\zeta(p, k, z) = \frac{\tilde{L}}{L + \tilde{L}} Q(p, k) e^{-qz} \quad z > 0, \quad (12)$$

$$\tilde{\zeta}(p, k, z) = -\frac{L}{L + \tilde{L}} Q(p, k) e^{qz} \quad z < 0, \quad (13)$$

where

$$L(p, k) = -\rho^{(0)} \frac{p^2 + v_A^2 k^2}{q(p, k)}. \quad (14)$$

Tilde indicates the same function evaluated for the lower half space. Because of the finite boundary layer at  $z = 0$ , the source function  $Q(p, k) = \zeta(p, k, 0) - \tilde{\zeta}(p, k, 0)$  is non-zero and can be found from the solution of the Riemann problem [1].

The expression for the displacement vector in the coordinate–time space can be found by using the so-called Cagniard–deHoop method [62, 63, 64, 59]. This method allows an analytical solution of the inverse Fourier transformation. The inverse Laplace transformation can be rewritten leading to an expression for the displacement vector as a convolution integral of the reconnection rate and an integration kernel in time, which can be solved numerically. After this procedure, the  $z$ -component of the displacement vector in coordinate–time space is found as

$$\zeta(x, z, t) = \frac{B}{\pi} \int_{\mathcal{C}} \Re \frac{\tilde{L}}{L + \tilde{L}} Q(s) F(t - \tau(s)) d\tau, \quad (15)$$

where  $F(t)$  is the reconnected flux,  $s = k/p$  and the integration is performed in the complex plane along a path  $\mathcal{C}$  where the integration variable  $\tau$  is real. From Eqs. 5–9 it is possible to derive the coordinate–time expressions for all relevant MHD parameters, like the pressure,

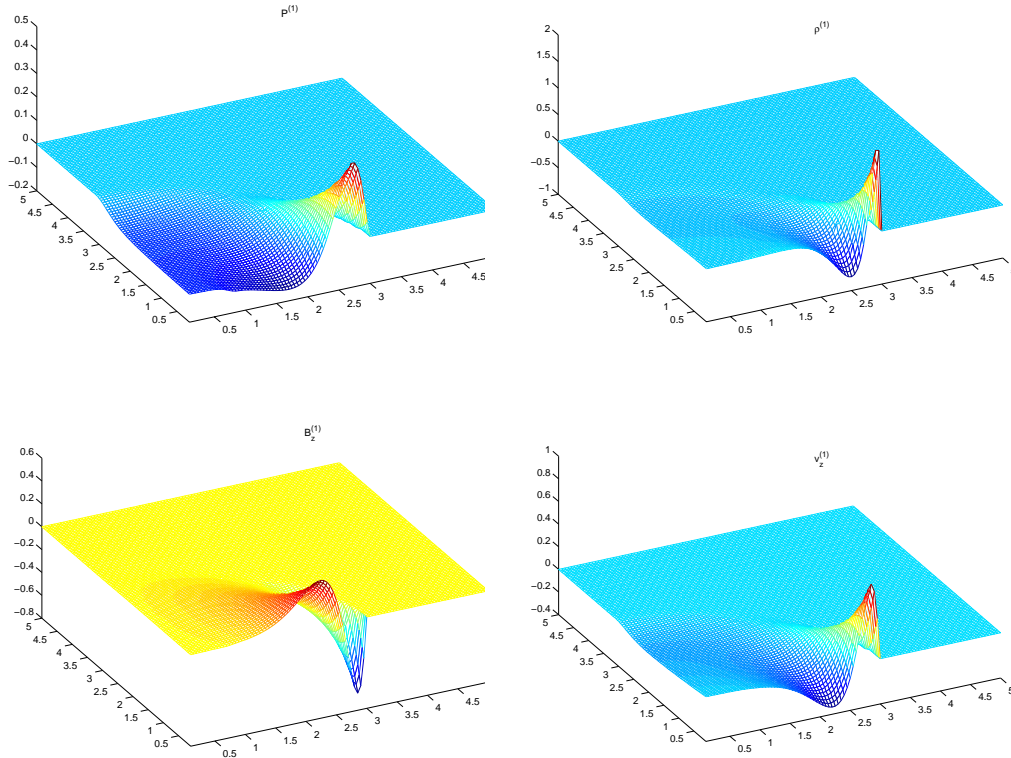


Figure 5. Variations of the total pressure (upper left panel), the plasma density (upper right panel), the  $z$ -component of the magnetic field (lower left panel), and the  $z$ -component of the flow velocity (lower right panel) for the upper half plane. The magnetic fields are  $B = 1$  and  $\tilde{B} = -1$ ,  $t = 3$ , and  $\beta = 0.1$ .

the plasma density, the magnetic field and the flow velocity for a given reconnection rate. The variation of the  $z$ -component of the magnetic field, which is used in the following for the reconstruction method, is given as

$$B_z^{(1)}(x, z, t) = \frac{B^2}{\pi} \int_C \Re \frac{\tilde{L}}{L + \tilde{L}} i s Q(s) E(t - \tau(s)) d\tau. \quad (16)$$

The expressions for the other quantities have a similar mathematical structure. In Fig. 5, the variations of the main MHD parameters are shown for fixed time ( $t = 3$ ) in the  $x$ - $z$ -plane. The reconnection rate is assumed to be

$$E(t) = \frac{b^2 e^2}{20} t^2 e^{-bt},$$

where  $b = 4$ .

It is possible to simulate magnetic field measurements along a satellite trajectory by using Eq. 16. Fig. 6 shows a time series of  $B_z^{(1)}$  measured by a satellite fixed in space. The characteristic asymmetric bipolar variation expected for the  $B_z$ -component is clearly visible,

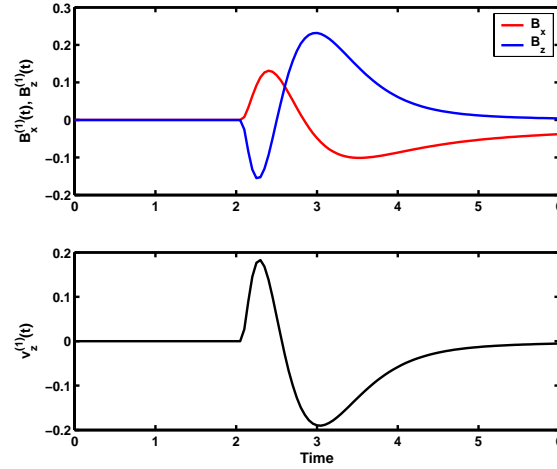


Figure 6. The normal ( $B_z$ ) and the tangential ( $B_x$ ) component of the magnetic field (upper panel) and the plasma flow velocity normal to the current sheet ( $v_z$ ; lower panel). All characteristic features expected for NFTEs, like the bipolar variation of  $B_z$  and the anticorrelated behavior of  $v_z$  can be seen.

and also the deflection of the x–component of the magnetic field. Additionally, the velocity behaves as proposed for NFTEs, with a upward flow of plasma followed by a strong flow directed downward to the plasma sheet.

#### 4. Solution of the Inverse Problem

Since we are interested to reconstruct the reconnection rate  $E(t)$  from satellite measurements of the magnetic field components, e.g.,  $B_z(t)$ , we have to solve an inverse problem. An inverse problem can be seen as a model of a phenomenon characterized by  $\varphi$ , which belongs to a certain space of models  $P$ . Furthermore, let  $u$  be the observed indirect attributes of the phenomenon with  $u \in U$ . An operator  $A$  relates the two values by

$$A\varphi = u. \quad (17)$$

As a rule, the  $\varphi$  attributes cannot be directly observed.

The main job when solving an inverse problem is to find out, whether the chosen model is compatible with the experimental data. The mathematical difficulty of solving such problems is that the inverse operator  $A^{-1}$  defined throughout its domain  $AP \subset U$  is not continuous. Hence there is the conventional division into the classes of well–posed and ill–posed problems. A well–posed problem, as defined by Hadamard [65], must meet the requirements that:

1. for each data set  $u$ , Eq. 17 is solvable in the entire space  $U$ ,
2. the solution is unique,

3. the solution is stable, meaning that small perturbations of  $u$  result in small perturbations of the solution  $\varphi$ .

If a problem does not meet one or more of these criteria, the problem is considered to be ill-posed. These kind of problems can be solved by using the theory of regularization, which we apply in the following.

To reconstruct the reconnection electric field from the magnetic field, we apply a Laplace transformation to the convolution integral (16) giving

$$B_z^{(1)}(p) = K(p)E(p), \quad (18)$$

where  $K(p)$  represents the kernel of the convolution integral (for convenience, the factor  $B^2/\pi$  in front of the integral in Eq. 16 is put into  $K(p)$ ). Thus, the reconnection electric field is given as  $E(p) = B_z^{(1)}(p)/K(p)$ . From this expression it is obvious that we are faced with an ill-posed inverse problem. If  $K(p) \rightarrow 0$ , requirement 1 is not fulfilled. Additionally, if  $K(p) \sim 0$ , small perturbations in the measured data  $B_z^{(1)}(p)$  will cause large perturbations in the result  $E(p)$ .

To avoid this problem, we introduce a regularization parameter  $M(p)$  [66] so that

$$E(p) = \frac{B_z^{(1)}(p)}{K(p) + M(p)}. \quad (19)$$

The regularization operator  $M(p)$  is defined as [67]

$$M(p) = \begin{cases} 0 & |p| < R_{max} \\ \infty & |p| > R_{max} \end{cases}. \quad (20)$$

This operator does not influence the electric field for small values of  $p$ , but when the functions tend to zero for large  $p$  ( $p > R_{max}$ ), the denominator goes to infinity, so that the reconnection electric field is zero in Laplace space and large oscillations are suppressed. The value of  $R_{max}$  is found from internal parameters of the numerical Laplace transformation.

## 5. Reconstruction of the Reconnection Rate and Site

After the observation of FTE signatures, several attempts were made to reconstruct and analyze different features of the reconnection process involved in the generation of FTEs. Southwood [68] predicted that FTE signatures would be observed by a satellite regardless of whether or not it actually penetrates the FTE. This suggestion was verified by Farrugia et al. [69], who reproduced the magnetic field signatures outside the flux tube by considering the flow of an inviscid, incompressible plasma over a semi-circular cylinder. In a new approach, Walthour et al. [70, 71] used a method based on integral transforms for inferring the cross-sectional size, shape, and the speed of propagation of a thin, infinitely long obstacle corresponding to a flux tube.

Another approach to this topic was used by several authors [72, 73, 74] who developed a method based on the Grad-Shafranov equation to reconstruct two-dimensional space

plasma structures in magnetohydrostatic equilibrium. Hu and Sonnerup [74] applied this model to two magnetopause crossings by the spacecraft AMPTE/IRM, and reconstructed magnetic field structures. Sonnerup et al. [75] used this method to give a rough estimation of the reconnection rate. However, the propagation of a reconnected flux tube can rather be described by the inertia force of the plasma and the Maxwellian tension, which is essentially a time-dependent process, and therefore this process can be hardly understood in a magnetohydrostatic approach.

Recently, different models based on multi-spacecraft measurements were developed to determine the position of the reconnection site with respect to the satellite. Wild et al. [76] used data from Cluster and Geotail positioned at the high- and the low-latitude dayside magnetopause. They consider the motion of reconnected flux tubes away from a user-defined location and compare the flux tube motion with the observed FTE-like signatures. In another approach, Fuselier et al. [77] determine the reconnection inflow velocity into the magnetosphere, and use Cluster and IMAGE data to estimate the approximate reconnection site. A third approach to reconstruct the reconnection rate, which was discussed above, was developed by Semenov et al. [67] for an incompressible plasma. It was applied to Cluster measurements in the magnetotail by Semenov et al. [48] and Penz et al. [49]. In the following, three applications of this method are presented.

### 5.1. Cluster Observations on September 8<sup>th</sup>, 2002

On September 8<sup>th</sup>, 2002, a favorable constellation of multiple spacecraft and ground-based observations allowed to reconstruct the time sequence of a substorm and to model the near-Earth magnetic configuration [35]. Between 20 and 23 UT, an isolated substorm with a peak AE of about 400 nT occurred. A clear growth phase was observed after the arrival of a southward-orientated IMF after 20 UT. The auroral breakup, the intensification of a westward electrojet, and Pi2 pulsations consistently indicated the expansion phase onset at 21:18 UT in the 22–24 MLT sector. The Cluster tetrahedron was centered in the middle of the magnetotail at  $[-16.7; 0.2; 4.5] R_e$  GSM. The satellites exited from the thinning plasma sheet shortly after 21:00 UT. Therefore, they were located outside of the plasma sheet at the time of interest. After 21:17 UT, a series of Earthward propagating 1 minute scale variations of the magnetic field and plasma flow components consistent with the picture of multiple NFTEs/flux ropes were observed (Fig. 7). The first NFTE appeared at about 21:17 UT and propagated Earthward at a speed  $v_x=625$  km/s;  $v_y=-72$  km/s (determined from timing of magnetic variations, [35]). After this NFTE, the plasma sheet continued to be thin for some 20 min until the transient plasma sheet expansions start to be observed. This is a favorable situation, because if the plasma sheet is thin, the approximation of a tangential discontinuity as an initial state is better justified.

Fig. 7 shows the measured  $B_x$ ,  $B_z$ , and  $v_z$  from the four Cluster satellites during the time interval from 21:16 to 21:26 UT. The GSM magnetic field data are obtained from the fluxgate magnetometer (FGM) experiment [78] with 1 s time resolution. The  $O^+$  moments with 4 s time resolution were measured by the Composition and Distribution Function Analyser (CODIF) of the Cluster Ion Spectrometry (CIS) experiment [79] observed at the Cluster spacecrafts. The  $O^+$  data was only used if the  $O^+$  density exceeded  $0.005 \text{ cm}^{-3}$ .

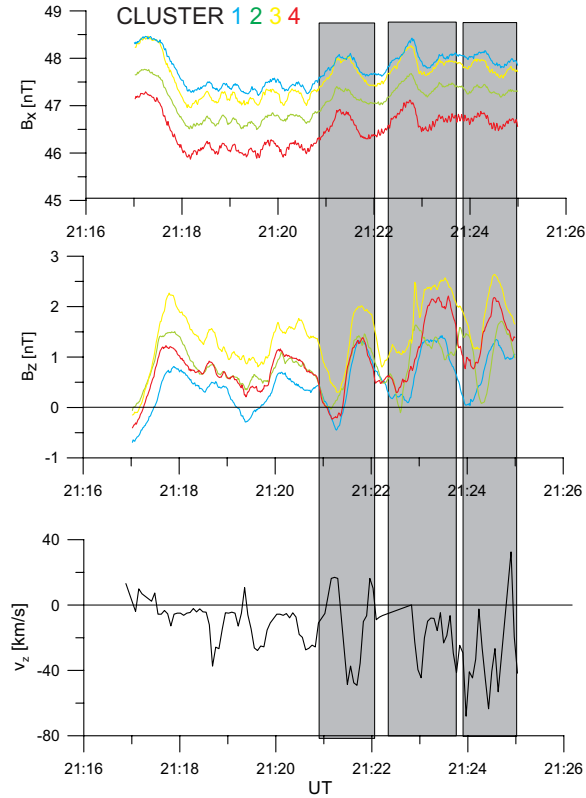


Figure 7. Cluster measurements of  $B_x$  (upper panel),  $B_z$  (middle panel), and  $v_z$  (lower panel). We analyze the NFTEs occurring at 21:21 UT, 21:22:30 UT, and 21:24 UT (shaded areas) [48].

We applied our model to the NFTEs starting at 21:21 UT, 21:22:30 UT, and 21:24 UT, ignoring the first NFTE at 21:17 UT (in which the interaction of reconnected flux tube with previously closed plasma sheet flux tubes should be more pronounced than in the following development). A comparison with the results of the theoretical model (Fig. 6) shows that the expected features for the perturbations are indeed found in the observations: the asymmetric bipolar variation of  $B_z$ , a compression of  $B_x$ , as well as a plasma flow  $v_z$  of cold  $O^+$  ions directed to the plasma sheet are clearly visible.

### 5.1.1. Reconstruction of the Events on September 8<sup>th</sup>, 2002

To evaluate the integration kernel  $K(p)$  we also need to know the spacecraft location with respect to the reconnection site (Fig. 8). Fortunately, the actual  $z$ -position of the neutral sheet (about  $+1 R_e$  in  $z$ -direction) is known from the modeling made in [35]. Therefore, the  $z$ -distance between the satellite and the reconnection site is approximately  $3.5 R_e$ .

The determination of the  $x$ -distance is done by using a global minimization routine. In

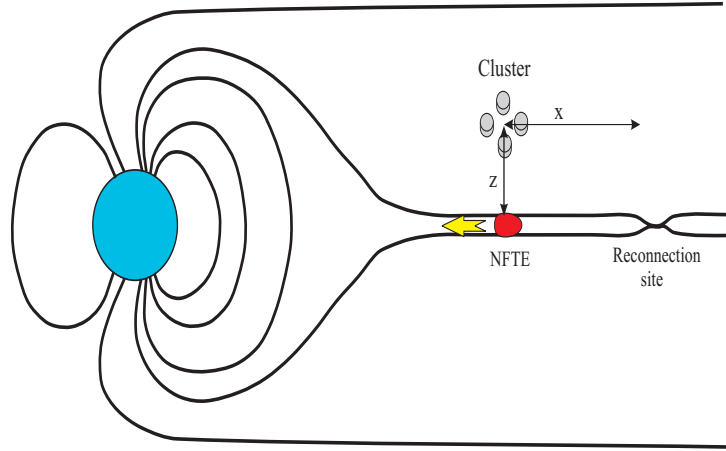


Figure 8. The position of the Cluster satellites with respect to the reconnection site. The  $z$ -distance is found from the modeling done by Sergeev et al. [35], while the  $x$ -distance is reconstructed by using a minimization routine.

our time-dependent model this is possible, because the shape of the shock is changing if the  $x$ -distance from the reconnection site is increasing. We use the measured  $B_z$  component as an input data, calculate the electric field in Laplace space, which should be strictly positive, but since we do not know the  $x$ -distance it can appear negative somewhere. Therefore, we take the module of the electric field and recalculate  $\tilde{B}_z$  out of it. This procedure can be summarized as

$$B_z(t) \Rightarrow B_z(p) \Rightarrow E(p) \Rightarrow E(t) \Rightarrow |E(t)| \Rightarrow \tilde{B}_z(t).$$

Then we minimize the difference between  $B_z(t)$  and  $\tilde{B}_z(t)$  with a least square approach in order to find the  $x$ -distance as the value of  $x$  where the difference between the initial and the reconstructed magnetic field has a minimum. We limit the search to distances less than  $35 R_e$ , which corresponds to the region of the near Earth neutral line (NENL), where reconnection most likely takes place. The local velocity of the disturbances is determined by using multipoint timing analysis [80], giving about 700 km/s. We assume that this velocity is approximately the Alfvén velocity. Additionally, this analysis shows that the propagation velocity is directed mainly Earthward in  $x$ -direction with a small  $y$ -component, which is a preferable configuration for our 2-D model. Now we know all quantities used for the normalization. Thus, we are able to analyze the events by using the method presented in the previous sections.

The reconnection electric field reconstructed for the NFTE starting at 21:21 UT in Fig. 7 is 1.1 mV/m over a time period of about 50 s from C1. C2 and C3 give a reconnection rate of 1.0 mV/m, while C4 gives 1.1 mV/m (Fig. 9).

The distance  $x$  between C1 and the reconnection site is  $8.6 R_e$ , so that the reconnection site is located at  $24.7 R_e$  in the magnetotail (Fig. 10). For C2,  $x = 8.6$ , giving  $24.9 R_e$  as the location of the reconnection site. From C3  $x$  is found to be 8.4, giving the reconnection

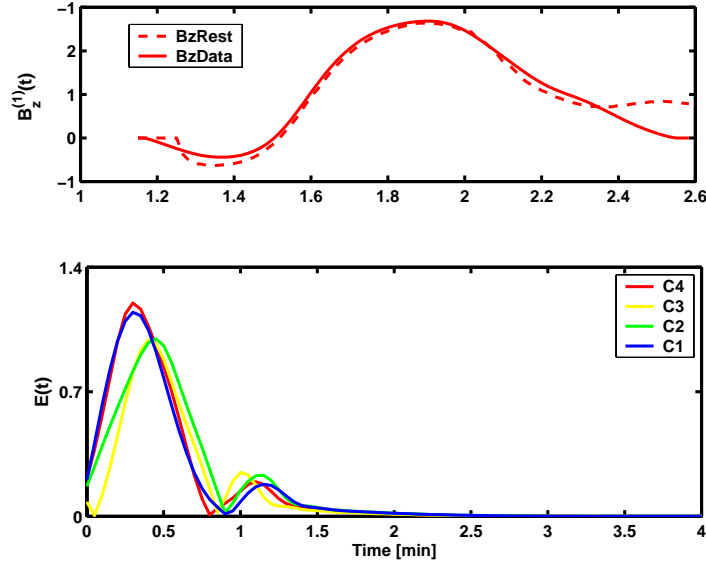


Figure 9. The lower panel shows the reconstructed reconnection rate from the four Cluster satellites, which has an amplitude of 1–1.1 mV/m and a duration of about 50 s. The upper panel shows a comparison between the measured  $B_z^{(1)}$  and the restored  $B_z^{(1)}$  from the reconstructed reconnection rate for C4.

site at  $24.6 R_e$ . C4 gives  $x = 7.6$ , corresponding to a reconnection site at  $24.3 R_e$ . One can see that the reconstructed amplitude of the reconnection electric field and the reconnection site are consistent among the four satellites. For example, C3 is located about  $0.5 R_e$  lower than C2, therefore the observed amplitude in the magnetic field perturbation at C3 is 1.7 nT compared with 1.3 nT at C2. Yet, the reconstructed amplitude of the electric field is quite similar, i.e., 1.0 mV/m from C3 and from C2. The same can be found for the  $x$ -distance, where C4 is located closest to the reconnection site, and therefore the model gives the smallest distance between the satellite and the reconnection site. Therefore our model shows that the observed features at all four satellites are associated with the same reconnection event.

Analysis of the event starting at 21:22:30 UT was done only with C2 and C4, since the other two satellites did not observe pronounced NFTE-like signatures. The reconnection rates are found to be 0.95 and 1.0 mV/m for C2 and C4, respectively. C2 gives  $x = 8.6$ , leading to a distance of  $24.9 R_e$  for the reconnection site. From C4,  $x$  is found to be  $8.25 R_e$ , giving a distance of  $24.8 R_e$  in the magnetotail. For the event starting at 21:24 UT, data from C2, C3, and C4 are used. The reconnection rate is found to be 0.95 mV/m (C2), 0.91 mV/m (C3), and 0.9 mV/m (C4). According to these data, the reconnection site is located at  $24.9 R_e$  (C2),  $23.9 R_e$  (C3), and  $24.5 R_e$  (C4) in the magnetotail.

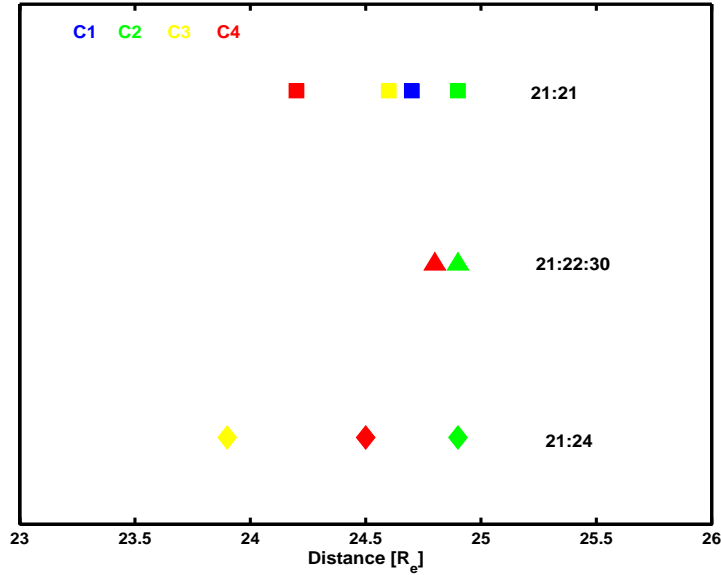


Figure 10. Location of the reconnection site reconstructed for the NFTE starting at 21:21 UT (squares), 21:22:30 UT (triangles), and 21:24 UT (diamonds) from the Cluster satellites.

## 6. Conclusion

We present a model to reconstruct the reconnection rate and the reconnection site from satellite measurements in a compressible plasma. As already predicted [48], the reconnection rate is smaller than inferred from the incompressible model. Also the distance between the reconnection site and the satellite decreased, while the duration of the pulses increase. All these features are consistent with the qualitative estimates done by Semenov et al. [48]. However, a significant reduction of the noise resulting from the solution of the inverse problem is achieved compared with the incompressible model [48]. Also the variations of the reconstructed reconnection rate and site between the satellites decreased.

Several simplifying assumptions were made to allow a treatment of the problem within an analytical model:

- *x*-distance: The *x*-distance between the satellite and the reconnection site is determined by using a minimization routine. There exists the possibility that more than one minimum occurs, meaning that there is no single solution for the problem considered. To avoid this problem, we applied our method only to the range of *x*-distances, where reconnection most likely takes place, namely to distances less than  $35 R_e$ , and run it with different starting points.
- Homogeneous background density : We assume that there is a homogeneous background density in the magnetotail. If the density changes significantly between the point of observation and the starting point of the disturbances, this will influence the propagation speed of the perturbations and may modify the results.

- Alfvén velocity: We assume that the perturbations in the magnetic field are moving approximately with Alfvén velocity. If the Alfvén velocity is not constant between the satellite and the reconnection site, the results will change. Since the Alfvén velocity is used for the normalization of the length scales, a variation of the Alfvén velocity will also give a variation of the spatial distances. If the Alfvén velocity decreases, also the length scales will decrease.

However, we found that the variations observed by the Cluster spacecrafts outside of the plasma sheet boundary are consistent with the impulsive model of magnetic reconnection used in this work. The characteristic bipolar variation of the  $B_z$ -component and the anti-correlated behavior of the perpendicular plasma flow velocity are reproduced. Application to NFTEs occurring on September 8<sup>th</sup>, 2002, gives an amplitude of the reconnection electric field in the range of 0.9–1.2 mV/m. This amplitude of the reconnection electric field is consistent with estimations of the magnetotail reconnection rate obtained from ground-based measurements [81, 82]. The time duration of the reconnection pulse is in the order of 50 s, while the reconnection site is located at about 23.9–24.9  $R_e$  tailwards.

### Acknowledgements

The authors thank A. Runov for fruitful discussions. This work is supported by the RFBR grants No. 04–05–64935 and No. 03–05–20012 BNTS, by the Austrian “Fonds zur Förderung der wissenschaftlichen Forschung” under project P17099–N08, by project No. I.12/04 from the “Österreichischer Austauschdienst”, and by INTAS Grant Nr. 03–51–3738. V.S.S. acknowledges financial support from the Technical University Graz and the hospitality of the Institut für Theoretische Physik during scientific visits to Graz. T.P. acknowledges support by the “Österreichische Forschungsgemeinschaft” and by a Paul-Urban scholarship from the Institute of Physics of the University of Graz during visits in St. Petersburg. V.V.I. acknowledges support by INTAS “Fellowship Grant for Young Scientists” Nr. 04–83–3816, and by the Nansen community. Also acknowledged is support by the Austrian Academy of Sciences, “Verwaltungsstelle für Auslandsbeziehungen”.

### References

- [1] Semenov, V. S.; Heyn, M. F.; Ivanov, I. B. *Phys. Plasmas* 2004, 11, 62–70.
- [2] Sweet, P. A. In *Electromagnetic Phenomena in Cosmic Physics*; Lehnert, B.; Ed.; Cambridge University Press: London, UK, 1958, pp 123–134.
- [3] Parker, E. N. *Astrophys. J. Suppl.* 1963, 8, 177–211.
- [4] Petschek, H. E. In *The Physics of Solar Flares*; Hess, W. N.; Ed.; NASA Spec. Publ.: Washington, DC, USA, 1964; SP–50, pp 425–440.
- [5] Erkaev, N. V.; Semenov, V. S.; Jamitzky, F. *Phys. Rev. Lett.* 2000, 84, 1455–1458.
- [6] Erkaev, N. V.; Semenov, V. S.; Alexeev, I. V.; Biernat, H. K. *Phys. Plasmas* 2001, 8, 4800–4809.

- 
- [7] Birn, J.; Drake, J. F.; Shay, M. A.; Rogers, B. N.; Denton, R. E.; Hesse, M.; Kuznetsova, M.; Ma, Z. W.; Bhattacharjee, A.; Otto, A.; Pritchett, P. L. *J. Geophys. Res.* 2001, 106, 3715–3720.
- [8] Phan, T. D. et al. *Nature* 2000, 404, 848–850.
- [9] Priest, E.; Forbes, T. *Magnetic Reconnection: MHD Theory and Applications*; Cambridge University Press: Cambridge, UK, 2000.
- [10] Paré, V. K. In *Magnetic reconnection in space and laboratory plasmas*; Hones, E. W.; Ed., Geophysical Monograph: Washington, DC, USA, 1984; 30, pp 341–346.
- [11] Yamada, M.; Levinton, F. M.; Pomphrey, N.; Budny, R.; Manickam, J.; Nagayama, Y. *Phys. Plasmas* 1994, 1, 3269–3276.
- [12] Yamada, M.; Ji, H.; Hsu, S.; Carter, T.; Kulsrud, R.; Bretz, N.; Jobes, F.; Ono, Y.; Perkins, F. *Phys. Plasmas* 1997, 4, 1936–1944.
- [13] Parker, E. N. *J. Geophys. Res.* 1957, 62, 509–520.
- [14] Scholer, M. *Lecture Notes in Physics* 2003, 612, 9–27.
- [15] Biernat, H. K.; Semenov, V. S.; Penz, T.; Miklenic, C.; Veronig, A.; Hanslmeier, A.; Vrsnak, B.; Heyn, M. F.; Ivanov, I. B.; Ivanova, V. V.; Kiehas, S.; Langmayr, D. *Hvar Obs. Bullet.* 2006, in press.
- [16] Uzdensky, D. A. *Astrophys. J.* 2003, 587, 450–457.
- [17] Axford, W. I.; McKenzie, J. F. *Astrophys. Space Sci.* 1996, 243, 1–4.
- [18] Mullan, D. J. In *The M-type stars*; Johnson, J. R.; Querci, F. R.; Ed.; NASA Spec. Publ: Washington, DC, USA 1986; SP-492, pp 455–479.
- [19] Verbunt, F. *Space Sci. Rev.* 1982, 32, 379–404.
- [20] Cowley, S. W. H. In *Magnetic Reconnection in Space and Laboratory Plasmas*; Hones, E. W.; Ed.; Geophysical Monograph: Washington, DC, USA, 1984; 30, pp 375–378.
- [21] Russell, C. T.; Elphic, R. C. *Space Sci. Rev.* 1978, 22, 681–715.
- [22] Haerendel, G.; Paschmann, G.; Sckopke, N.; Rosenbauer, H.; Hedgecock, P. C. *J. Geophys. Res.* 1978, 83, 3195–3216.
- [23] Rijnbeek, R. P.; Cowley, S. W. H.; Southwood, D. J.; Russell, C. T. *J. Geophys. Res.* 1984, 89, 786–800.
- [24] Kawano, H.; Russell, C. T. *J. Geophys. Res.* 1997, 102, 11307–11314.
- [25] Twitty, C.; Phan, T. D.; Paschmann, G.; Lavraud, B.; Rème, H.; Dunlop, M. *Geophys. Res. Lett.* 2004, 31, L19808, doi:10.1029/2004GL020646.

- 
- [26] Frey, H. U.; Phan, T. D.; Fuselier, S. A.; Mende, S. B. *Nature* 2003, 426, 533–537.
- [27] Walker, R. J.; Ogino, T.; Raeder, J.; Ashour–Abdalla, M. J. *Geophys. Res.* 1993, 98, 17235–17250.
- [28] Lopez, R. E.; Benitez–Marquez, E.; Wiltberger, M. J.; Lyon, J. G.; Figueroa, R. *Adv. Space Res.* 2003, 31, 1167–1176.
- [29] Sergeev, V. A.; Semenov, V. S.; Sidneva, M. V. *Planet. Space Sci.* 1987, 35, 1199–1212.
- [30] Sergeev, V. A.; Elphic, R. C.; Mozer, F. S.; Saint–Marc, A.; Sauvaud, J. A. *Planet. Space Sci.* 1992, 40, 1551–1572.
- [31] Ieda, A.; Machida, S.; Mukai, T.; Saito, Y.; Yamamoto, T.; Nishida, A.; Terasawa, T.; Kokubun, S. J. *Geophys. Res.* 1998, 103, 4453–4465.
- [32] Slavin, J. A.; Lepping, R. P.; Gjerloev, J.; Fairfield, D. H.; Hesse, M.; Owen, C. J.; Moldwin, M. B.; Nagai, T.; Ieda, A.; Mukai, T. J. *Geophys. Res.* 2003, 108, 1015, doi:10.1029/2002JA009557.
- [33] Nagai, T.; Shinohara, I.; Fujimoto, M.; Hoshino, M.; Saito, Y.; Machida, S.; Mukai, T. J. *Geophys. Res.* 2001, 106, 25929–25950.
- [34] Runov, A.; Nakamura, R.; Baumjohann, W.; Treumann, R. A.; Zhang, T. L.; Volwerk, M.; Vörös, Z.; Balogh, A.; Glassmeier, K.–H.; Klecker, B.; Rème, H.; Kistler, L. *Geophys. Res. Lett.* 2003, 30, 1579, doi:10.1029/2002GL016730.
- [35] Sergeev, V. A.; Kubyshkina, M. V.; Baumjohann, W.; Nakamura, R.; Amm, O.; Pulkkinen, T.; Angelopoulos, V.; Mende, S. B.; Klecker, B.; Nagai, T.; Sauvaud, J.–A.; Slavin, J. A.; Thomsen, M. F. *Ann. Geophys.* 2005, in press.
- [36] Kistler, L.; Mouikis, C.; Moebius, E.; Klecker, B.; Sauvaud, J.–A.; Rème, H.; Korth, A.; Marocci, M.; Lundin, R.; Parks, G.; Balogh, A. J. *Geophys. Res.* 2005, 110, A06213, doi:10.1029/2004JA010653.
- [37] Wygant, J. R.; Cattell, C. A.; Lysak, R.; Song, Y.; Dombeck, J.; McFadden, J.; Mozer, F. S.; Carlson, C.; Parks, G.; Lucek, E. A.; Balogh, A.; Andre, M.; Rème, H.; Hesse, M.; Mouikis, C. J. *Geophys. Res.* 2005, submitted.
- [38] Cattell, C.; Dombeck, J.; Wygant, J.; Drake, J. F.; Swisdak, M.; Goldstein, M. L.; Keith, W.; Fazakerley, A.; Andre, M.; Lucek, E.; Balogh, A. J. *Geophys. Res.* 2005, 110, A01211, 10.1029/2004JA010519.
- [39] Nakamura, R.; Baumjohann, W.; Nagai, T.; Fujimoto, M.; Mukai, T.; Klecker, B.; Treumann, R. A.; Balogh, A.; Rème, H.; Sauvaud, J.–A.; Kistler, L.; Mouikis, C.; Owen, C. J.; Fazakerley, A.; Dewhurst, J.; Bogdanova, Y. J. *Geophys. Res.* 2004, 109, A05204, doi:10.1029/2003JA010174.

- [40] Alexeev, I. V.; Owen, C. J.; Fazakerley, A. N.; Runov, A.; Dewhurst, J.; Balogh, A.; Rème, H.; Klecker, B.; Kistler, L. *Geophys. Res. Lett.* 2005, 32, L03101, doi:10.1029/2004GL021420.
- [41] Asano, Y.; Nakamura, R.; Baumjohann, W.; Runov, A.; Vörös, Z.; Volwerk, M.; Zhang, T. L. *Geophys. Res. Lett.* 2005, 32, L03108, doi:10.1029/2004GL021834.
- [42] Treumann, R. A.; Jaroschek, C. H.; Nakamura, R.; Runov, A.; Scholer, M. *COSPAR Colloquia Series*, 2005, in press.
- [43] Eriksson, S.; Oieroset, M.; Baker, D.; Mouikis, C.; Vaivads, A.; Dunlop, M.; Rème, H.; Ergun, R.; Balogh, A. J. *Geophys. Res.* 2004, 109, A05212, doi:10.1029/2003JA010534.
- [44] Slavin, J. A.; Lepping, R.; Gjerloev, J.; Fairfield, D.; Acuna, M.; Goldstein, M.; Balogh, A.; Dunlop, M.; Kivelson, M.; Khurana, K.; Fazakerley, A.; Owen, C. J.; Rème, H.; Bosqued J. *Geophys. Res. Lett.* 2003, 30, 1362, doi:10.1029/2003GL016411.
- [45] Zong, Q.-G.; Fritz, T. A.; Pu, Z. Y.; Fu, S. Y.; Baker, D. N.; Zhang, H.; Lui, A. T.; Vogiatzis, I.; Glassmeier, K.-H.; Korth, A.; Daly, P. W.; Balogh, A.; Rème, H. *Geophys. Res. Lett.* 2004, 31, L18803, doi:10.1029/2004GL020692.
- [46] Slavin, J. A.; Owen, C. J.; Dunlop, M. W.; Boralev, E.; Moldwin, M. B.; Sibeck, D. G.; Tanskanen, E.; Goldstein, M. L.; Fazaderley, A.; Balogh, A.; Lucek, E.; Richter, I.; Rème, H.; Bosqued, J. *Geophys. Res. Lett.* 2003, 30, 2208, doi:10.1029/2003GL018438.
- [47] Owen, C. J.; Slavin, J. A.; Fazakerley, A. N.; Dunlop, M. W.; Balogh, A. *Geophys. Res. Lett.* 2005, 32, L03104, doi:10.1029/2004GL021767.
- [48] Semenov, V. S.; Penz, T.; Ivanova, V. V.; Sergeev, V. A.; Biernat, H. K.; Nakamura, R.; Heyn, M. F.; Kubyshkin, I. V.; Ivanov, I. B. *J. Geophys. Res.* 2005, 110, A11217, doi:10.1029/2005JA011181.
- [49] Penz, T.; Semenov, V. S.; Ivanova, V. V.; Biernat, H. K.; Sergeev, V. A.; Nakamura, R.; Kubyshkin, I. V.; Ivanov, I. B.; Heyn, M. F. *Adv. Space Res.* 2006, in press.
- [50] Nakamura, R.; Baumjohann, W.; Mouikis, C.; Kistler, L. M.; Runov, A.; Volwerk, M.; Asano, Y.; Vörös, Z.; Zhang, T. L.; Klecker, B.; Rème, H.; Balogh, A. *Geophys. Res. Lett.* 2004, 31, L09804, doi:10.1029/2004GL019558.
- [51] Nakamura, R.; Baumjohann, W.; Klecker, B.; Bogdanova, Y.; Balogh, A.; Rème, H.; Bosqued, J.-M.; Dandouras, I.; Sauvaud, J.-A.; Glassmeier, K.-H.; Kistler, L.; Mouikis, C.; Zhang, T. L.; Eichelberger, H.; Runov, A. *Geophys. Res. Lett.* 2002, 29, 1942, doi:10.1029/2002GL015763.
- [52] Volwerk, M.; Nakamura, R.; Baumjohann, W.; Treumann, R. A.; Runov, A.; Vörös, Z.; Zhang, T. L.; Asano, Y.; Klecker, B.; Richter, I.; Balogh, A.; Rème, H. *J. Geophys. Res.* 2003, 108, 1429, doi:10.1029/2003JA010155.

- [53] Vörös, Z.; Baumjohann, W.; Nakamura, R.; Runov, A.; Zhang, T. L.; Volwerk, M.; Eichelberger, H.; Balogh, A.; Horbury, T. S.; Glassmeier, K.-H.; Klecker, B.; Rème, H. *Ann. Geophys.* 2003, 21, 1955–1964.
- [54] Grocott, A.; Yeoman, T.; Nakamura, R.; Cowley, S. W. H.; Frey, H.; Rème, H.; Klecker, B. *Ann. Geophys.* 2004, 22, 1061–1075.
- [55] Nakamura, R.; Amm, O.; Laakso, H.; Draper, N.; Lester, M.; Grocott, A.; Klecker, B.; McCrea, I.; Balogh, A.; Rème, H.; Andre, M. *Ann. Geophys.* 2005, 99, 553–566.
- [56] Biernat, H. K.; Heyn, M. F.; Semenov, V. S. *J. Geophys. Res.* 1987, 92, 3392–3396.
- [57] Semenov, V. S.; Kubyshkin, I. V.; Lebedeva, V. V.; Rijnbeek, R. P.; Heyn, M. F.; Biernat, H. K.; Farrugia, C. J. *Planet. Space Sci.* 1992, 40, 63–87.
- [58] Semenov, V. S.; Kubyshkin, I. V.; Rijnbeek, R. P.; Biernat, H. K. In *Physics of magnetic reconnection in high-temperature plasmas*; Ugai, M.; Ed.; Research Signpost: Trivandrum, India, 2004, pp 35–68.
- [59] Heyn, M. F.; Semenov, V. S. *Phys. Plasmas* 1996, 3, 2725–2741.
- [60] Heyn, M. F.; Biernat, H. K.; Rijnbeek, R. P.; Semenov, V. S. *J. Plasma Physics* 1988, 40, 235–252.
- [61] Akhiezer, A. I.; Akhiezer, I. A.; Polovin, R. V.; Sitenko, A. G.; Stepanov, K. N. *Plasma Electrodynamics*; Pergamon Press: Oxford, UK, 1975.
- [62] Lamb, H. *Philos. Trans. R. Soc. London Ser. A* 1904, 203, 1–42.
- [63] Cagniard, L. *Reflexion et Refraction des Ondes Seismiques Progressive*; Gauthier-Villard: Paris, France, 1939; English translation by Flinn, E. A.; Dix, C. H. *Reflection and refraction of progressive seismic waves*; McGraw-Hill: New York, USA, 1962.
- [64] deHoop, A. T. *Appl. Sci. Res. B* 1960, 8, 349–356.
- [65] Hadamard, J. *Le problème de Cauchy et les équations aux dérivées partielles Lineaires Hyperboliques*; Hermann: Paris, France, 1932.
- [66] Tikhonov, A. N.; Arsenin, V. Y. *Solutions of ill-posed problems*; John Wiley: New York, USA, 1977.
- [67] Semenov, V. S.; Penz, T.; Heyn, M. F.; Ivanov, I. B.; Kubyshkin, I. V.; Biernat, H. K.; Ivanova, V. V. In *Solar-planetary relations*; Biernat, H. K.; Lammer, H.; Vogl, D. F.; Mühlbacher, S.; Eds.; Research Signpost: Trivandrum, India, 2005, pp 261–302.
- [68] Southwood, D. J. *Adv. Space Res.* 1985, 5, 7–14.
- [69] Farrugia, C. J.; Elphic, R. C.; Southwood, D. J.; Cowley, S. W. H. *Planet. Space Sci.* 1987, 35, 227–240.
- [70] Walthour, D. W.; Sonnerup, B. U. Ö.; Paschmann, G.; Lühr, H.; Klumpar, D.; Potemra, T. J. *Geophys. Res.* 1993, 98, 1489–1504.

- 
- [71] Walthour, D. W.; Sonnerup, B. U. Ö.; Elphic, R. C.; Russell, C. T. *J. Geophys. Res.* 1994, 99, 8555–8563.
- [72] Hau, L.-N.; Sonnerup, B. U. Ö. *J. Geophys. Res.* 1999, 104, 6899–6918.
- [73] Hu, Q.; Sonnerup, B. U. Ö. *Geophys. Res. Lett.* 2001, 28, 467–470.
- [74] Hu, Q.; Sonnerup, B. U. Ö. *J. Geophys. Res.* 2003, 108, 1011, doi:10.1029/2002JA009323.
- [75] Sonnerup, B. U. Ö.; Hasegawa, H.; Paschmann, G. *Geophys. Res. Lett.* 2004, 31, L11803, doi:10.1029/2004GL020134.
- [76] Wild, J. A.; Milan, S. E.; Cowley, S. W. H.; Bosqued, J. M.; Rème, H.; Nagai, T.; Kokubun, S.; Saito, Y.; Mukai, T.; Davies, J. A.; Cooling, B. M. A.; Balogh, A.; Daly, P. W. *Ann. Geophys.* 2005, 23, 445–460.
- [77] Fuselier, S. A.; Trattner, K. J.; Petrinec, S. M.; Owen, C. J.; Rème, H. *J. Geophys. Res.* 2005, 110, A06212, doi:10.1029/2004JA010805.
- [78] Balogh, A. et al. *Ann. Geophys.* 2001, 19, 1207–1217.
- [79] Rème, H. et al. *Ann. Geophys.* 2001, 19, 1303–1354.
- [80] Harvey, C. C. In *Analysis methods for multi-spacecraft data*; Paschmann, G.; Daly, P. W.; Eds.; ISSI SR-001, 1998.
- [81] Blanchard, G. T.; Lyons, L. R.; de la Beaujardière, O.; Doe, R. A.; Mendillo, M. J. *Geophys. Res.* 1996, 101, 15265–15276.
- [82] Østgaard, N.; Moen, J.; Mende, S. B.; Frey, H. U.; Immel, T. J.; Gallop, P.; Oksavik, K.; Fujimoto, M. *Ann. Geophys.* 2005, 23, 123–134.